

See discussions, stats, and author profiles for this publication at: <https://www.researchgate.net/publication/323756176>

# Microstructural and mechanical characterization of electroplated nickel matrix composite coatings

Article in *Surface Engineering* · April 2018

DOI: 10.1080/02670844.2018.1433270

CITATIONS

23

READS

852

5 authors, including:



[David Mercier](#)

ANSYS

82 PUBLICATIONS 660 CITATIONS

[SEE PROFILE](#)



[Matteo Caruso](#)

Laborelec

20 PUBLICATIONS 155 CITATIONS

[SEE PROFILE](#)



[Jean-Francois Vanhumbeeck](#)

CRM Group

22 PUBLICATIONS 340 CITATIONS

[SEE PROFILE](#)

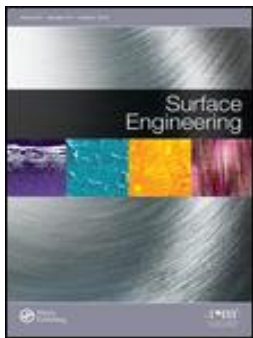


[Xavier Vanden Eynde](#)

CRM Group

88 PUBLICATIONS 892 CITATIONS

[SEE PROFILE](#)



## Microstructural and mechanical characterisation of electroplated nickel matrix composite coatings

David Mercier, Jean-François Vanhumbeeck, Matteo Caruso, Xavier Vanden Eynde & Mickaël Febvre

To cite this article: David Mercier, Jean-François Vanhumbeeck, Matteo Caruso, Xavier Vanden Eynde & Mickaël Febvre (2018): Microstructural and mechanical characterisation of electroplated nickel matrix composite coatings, Surface Engineering, DOI: [10.1080/02670844.2018.1433270](https://doi.org/10.1080/02670844.2018.1433270)

To link to this article: <https://doi.org/10.1080/02670844.2018.1433270>



Published online: 12 Apr 2018.



Submit your article to this journal [↗](#)





View related articles [↗](#)



View Crossmark data [↗](#)



# Microstructural and mechanical characterisation of electroplated nickel matrix composite coatings

David Mercier <sup>a</sup>, Jean-François Vanhumbecq<sup>a</sup>, Matteo Caruso<sup>a</sup>, Xavier Vanden Eynde <sup>a</sup> and Mickaël Febvre<sup>b</sup>

<sup>a</sup>CRM Group, Liege, Belgium; <sup>b</sup>Bruker Nano Surface Division, Palaiseau, France

## ABSTRACT

Metal matrix composite coatings reinforced with hard ceramic particles are attracting growing interest due to their promising mechanical properties. In the present work, a thick nickel coating, containing micrometric Silicon Carbide (SiC) particles, was electro-deposited on a steel substrate from a suspension of SiC in a Watts-type Ni-plating bath. The texture and microstructure of the coating were examined using electron backscatter diffraction combined with energy-dispersive spectroscopy for phase differentiation. The interfacial strength between the Ni matrix and the SiC particles was investigated by nanoscratch experiments. Grid nanoindentation technique coupled with an image correlation-based targeted indentation analysis and a statistical data treatment were employed to quantify mechanical properties of the composite and to map and extract mechanical properties and fractions of each phase. Additional investigation of the mechanical properties of the coating was performed using peak force quantitative nanomechanical mapping experiments.

## ARTICLE HISTORY

Received 4 August 2017  
Revised 21 December 2017  
Accepted 22 January 2018

## KEYWORDS

Electroplating; particle-reinforced metallic matrix coating; Ni-SiC; nanoindentation; mechanical property mapping; image correlation; peak force quantitative nanomechanical mapping experiment

## Nomenclature

ND normal direction  
CSM continuous stiffness measurement

## Introduction

Metal matrix composite coatings reinforced with ceramic particles [1–3] or graphene [4] have very interesting mechanical properties arising from the combination of a more ductile matrix with harder reinforcing particles. Our work is focused on electroplated composite coatings, combining a Ni matrix with SiC particles [5–9]. This combination allows getting at the same time a good protection against corrosion and good wear resistance, two properties of primary importance for mechanical applications. The first electroplated matrix composite coatings were developed in the 1960s, mainly to protect parts of the thermal motor against wear. Numerous scientific papers are devoted to this technology as well as patents, especially by engine manufacturers (e.g. Honda, Toyota, Suzuki, Kawasaki, and Mitsubishi) as published in [10]. In recent years, these coatings arouse interest among industrials as a wear-resistant coating for hard chromium substitution. Owing to their micro-composite nature, the assessment of the mechanical and microstructural characteristics of the coating itself and of each phase (matrix and particles) requires appropriate procedures. Several approaches were proposed in the literature. For instance, microstructural characterisations by EBSD allow assessing the matrix and particles

grain size as well as the phase fractions [11]. The interface between metallic matrix and hard particles has a great deal of importance in defining the macroscopic properties of the composite material [12] and can be mechanically characterised using nanoscratch experiments according to Pöhl et al. [13]. Nanoindentation technique can also be used to extract mean elastic modulus and hardness values of the coating [14,15], or for mechanical property mapping and statistical estimation of each phase of the PRMMC [16–22]. Moreover, nanoindentation mapping is sometimes coupled with other techniques like energy-dispersive spectroscopy (EDS) to correlate mechanical behaviour with chemical or microstructural answer [23]. Finally, peak force quantitative nanomechanical mapping (PF-QNM) atomic force microscopy (AFM)-based experiment was also demonstrated to be suitable for assessing the mechanical behaviour of each phase [24–26].

In the present article, a complementary methodology is proposed for the microstructural and mechanical characterisation of a PRMMC coating, based on the combination of EDS, EBSD, nanoscratch and nanoindentation experiments. First, the preparation of the metallic matrix composite sample is described, together with the applied characterisation procedures. Then, results of the microstructural analysis, obtained by EBSD coupled with EDS and AFM, are presented and discussed. Interface strength and mechanical properties of the coating and of each phase are characterised, respectively, by nanoscratch and nanoindentation

techniques. Phase fractions and mechanical property values are then extracted from grid nanoindentation experiments using innovative and quantitative statistical treatments of datasets, with image correlation-based targeted indentation (ICBTI) analysis and with multi-Gaussian deconvolution of mechanical property distributions. Finally, the capabilities of AFM measurement for mechanical characterisation of such coating are investigated and discussed.

## Experimental

### Material and experimental methods

For this study, an electroplated composite coating, combining a metallic matrix with a second ceramic phase, has been applied on a DC01 steel substrate, from a Watts-type Ni-plating bath with the addition of 50 g/L of SiC particles (Starck  $\alpha$ -SiC Grade UF-05, mean granulometry about 2  $\mu\text{m}$ ). Particles are maintained in suspension in the bath by mean of a suitable stirring system. This coating was deposited under direct current with a current density of 5 A/dm<sup>2</sup>. A Ni reference sample was also prepared under the same conditions as the composite coating, without SiC particles in the bath. The latter was used as a reference sample for the indentation tests in order to extract the mechanical properties of pure Ni layer. Similarly, a bulk  $\alpha$ -SiC sample was used as a reference for the SiC phase.

### Experimental methods

Cross-section of the coating was observed by scanning electron microscopy (SEM) (JEOL JSM 7001F), to quantify coating thickness and based on complementary image analyses, surface fractions of Ni and SiC phases along the coating thickness. Texture and microstructure of the coating top surface have been characterised, in order to differentiate the phases in presence, by combining EBSD data using an EDAX TSL camera and with EDS data obtained using an EDAX SDD Apollo XPP detector. Both analyzers are fixed to our JEOL 7001F system. For this, sample surface has been carefully prepared by successive mechanical and chemical polishing steps. Final polishing was carried out using a standard OP-U solution (colloidal silica suspension) to remove the work-hardened top layer. The latter preparation step was essential for avoiding artefacts of preparation. Surface microstructure and surface topography were also characterised, respectively, by optical microscopy (OM) (Olympus AX-70), and by AFM with a Bruker Dimension Icon AFM, to confirm experimental results obtained from EBSD-EDS.

Mechanical characterisation of the Ni/SiC interface inside the coating was performed through nanoscratch

experiments with a sphero-conical indenter (5  $\mu\text{m}$  / 90°) (Agilent Nano Indenter G200 – XP head). 10 nanoscratches were performed on the coating surface to have a statistical overview of the mechanical and tribological behaviours of the coating. The maximum applied load is 200 mN and the scratch length is 200  $\mu\text{m}$ . Horizontal displacement of the indenter is set to a speed of scratch of 5  $\mu\text{m/s}$ . Surface profiles before and after scratching are carried out at a scanning speed of 5  $\mu\text{m/s}$  and a load of 50  $\mu\text{N}$ . The mechanical strength of particles/matrix interface was qualified from the correlation between optical microscopic observations with grooves profiles from the nanoscratch test.

Mechanical properties of the coating (and of the Ni and SiC reference samples) were characterised by Berkovich nanoindentation tests (Agilent Nano Indenter G200 - XP head), using the method from Oliver and Pharr [14]. The Berkovich indenter was in diamond with a 20 nm nominal tip radius curvature. All nanoindentation tests consisted of loading the indenter at a constant normalised strain rate of 0.05 s<sup>-1</sup>, to a prescribed depth (100 nm or 2  $\mu\text{m}$ ), and then unloading under the same conditions. Indentation experiments were performed at room temperature, under the continuous stiffness measurement (CSM) mode. The CSM oscillations were set to an average amplitude of 2 nm and at a frequency of 45 Hz. A first grid of indents (6  $\times$  6 matrix, 2  $\mu\text{m}$  deep, 50  $\mu\text{m}$  horizontal and vertical spacing), was made to estimate the average composite hardness and elastic modulus values of the coating. A second set of nanoindents (25  $\times$  25 matrix, 100 nm indentation depth, 2  $\mu\text{m}$  vertical and horizontal spacing) was also performed to map the mechanical properties of the top surface of the PRMMC coating and to assess statistically the average values of hardness and elastic modulus of each phase (Ni and SiC). The indentation depth of 100 nm has been selected for the second indentation grid, in order to fulfil the criterion proposed by Constantinides et al. [17], namely that maximum indentation depth should be less than 10% of the particle size. For both grids, spacing between nanoindents is at least 2 times the mean size of the zone below the indent (3 times the penetration depth in the case of Berkovich indentation), to avoid interference of neighbours indents.

Finally, mechanical behaviour of each phase in the PRMMC coating was investigated through PF-QNM AFM-based experiment (Bruker Dimension Icon AFM). PF-QNM trials were carried out using a steel cantilever (spring constant about 400 N/m) with glued Berkovich diamond tip. 50  $\times$  50  $\mu\text{m}$  nanomechanical maps were recorded, with 512  $\times$  512 data points. This technique allows measuring the local nanomechanical properties with the same lateral nanometric resolution as in the topographical image mode.

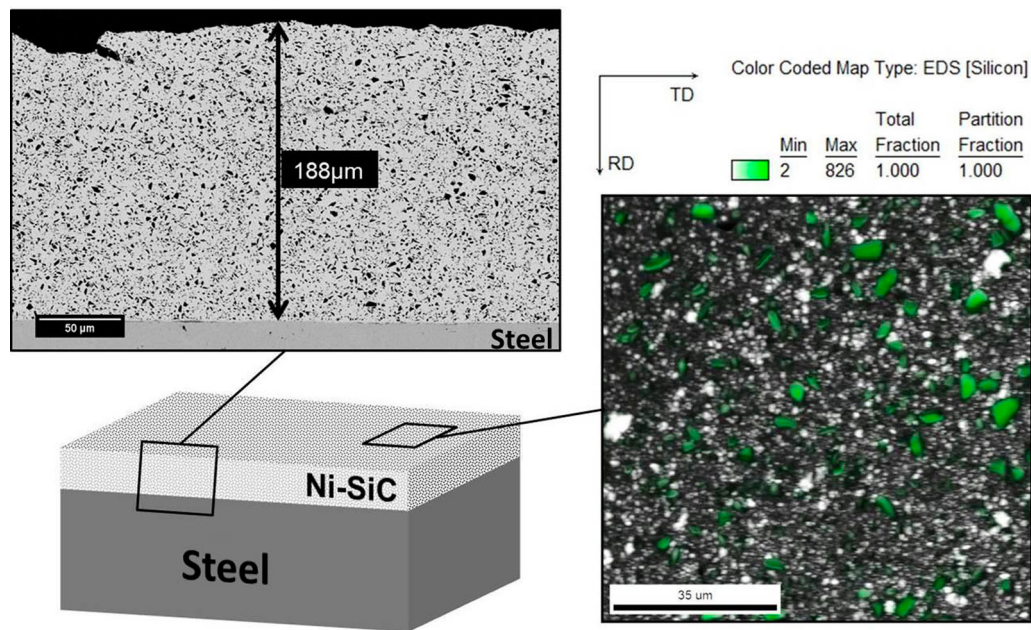


**Figure 1.** Illustration of morphological and microstructural properties of the Ni-SiC coating.

## Results and discussion

### Microstructural characterisation of Ni-SiC coating

SEM cross-sectional observation of the Ni-SiC coating demonstrates a very homogeneous distribution of the ceramic phase in the matrix. Average film thickness was measured to be  $(176 \pm 15) \mu\text{m}$  (Figure 1 right image with (SiC particle in green based on Si EDS signal)). The overlay of the EBSD quality index image and Si EDS maps allows distinguishing easily between the Ni matrix (face-centred cubic) from SiC particles (hexagonal) (Figure 1). Once the SiC phase was located, EBSD dataset was cleaned by subtracting the raw data corresponding to the ceramic phase, to map only the Ni matrix. Using this approach, it was possible

to determine microstructural characteristics of each phase independently. Grain sizes of about  $(0.34 \pm 0.27) \mu\text{m}$  and  $(1.13 \pm 0.16) \mu\text{m}$  were estimated, respectively, for the Ni and/or SiC particles (Figure 2). From the inverse pole figures shown in Figure 2, a weak texture is found for the Ni grains in the coating. Ni grains oriented along the  $\langle 001 \rangle$  direction, parallel to ND, are 1.5x more present than in a random distribution. Surface fraction values of the two phases are estimated from the different microscopic observations (Table 1). In the case of SEM and OM observations, an image analysis by thresholding of the grey levels was carried out, while phases were differentiated based on EBSD images, using EDS measurements. A good agreement between the different methods for phase fraction estimations was found in both cases, with a Ni-SiC ratio

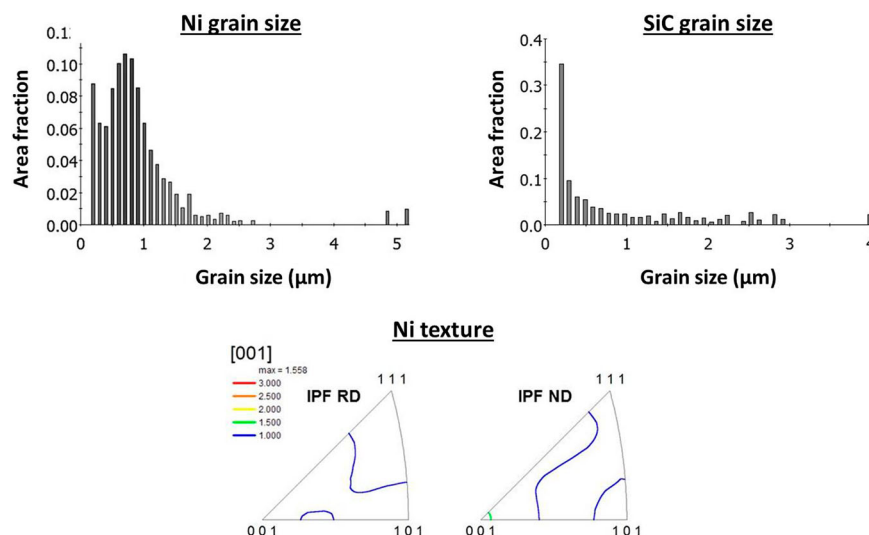


**Figure 2.** Ni and SiC grain sizes and Ni texture, as extracted from EBSD measurements.



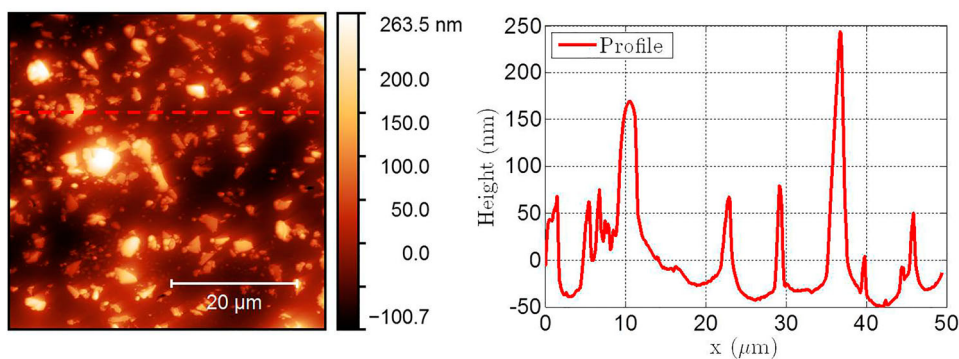
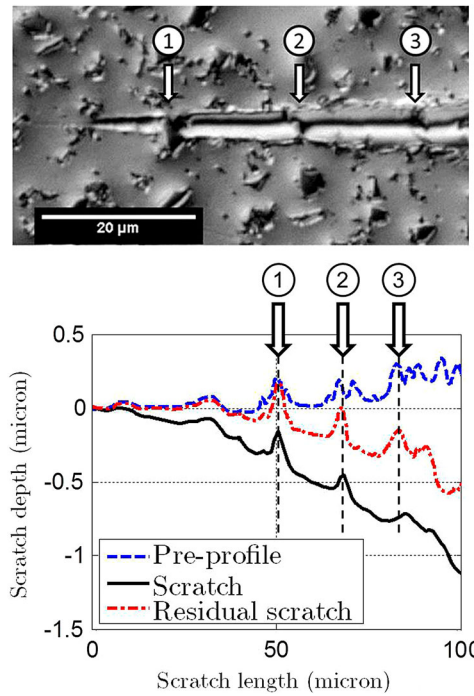
**Table 1.** Surface fractions of Ni and SiC obtained from microscopic observations.

	Ni	SiC
Surface phase fraction (SEM)	$(81.7 \pm 1.2)\%$	$(18.3 \pm 1.4)\%$
Cross-sectional view		
Surface phase fraction (OM)	$(79.9 \pm 1.8)\%$	$(20.1 \pm 1.9)\%$
Top view		
Surface phase fraction (EBSD)	$(79.9 \pm 5.0)\%$	$(20.1 \pm 5.3)\%$
Top view		

about 80/20 (Table 1). The AFM micrograph of the PRMMC coating surface is shown in Figure 3 and the average surface roughness ( $R_a$ ) is around 43.9 nm, with a peak to valley about 405 nm. It is clear from AFM measurement that, despite the careful polishing procedure, the coating surface is not perfectly smooth as a consequence of the presence of prominent SiC particles. This topography can raise issues for the following nanomechanical tests.

### Mechanical characterisation of Ni/SiC interface

Qualification of the mechanical strength of the Ni/SiC interface was based on the analysis of nanoscratch experiments performed on the composite coating. A typical scratch groove from this test is shown in Figure 4, together with the associated transverse profiles measured before (initial topography), during and after (residual groove) scratching step. As indicated by the optical image, the shape of the groove is well defined and mainly controlled by a ploughing-type plastic deformation of the Ni matrix. In addition, it is noted that three SiC particles (indexed 1–3 in Figure 4) visible on the post-mortem optical micrograph of the groove are also observable in the different profiles. The levels of normal load at these positions are, respectively, about 95, 130 and 160 mN, corresponding to mean normal contact pressures of 17.4, 12.4 and 10.1 GPa, obtained under the assumptions and the approach established by Beake et al. [27]. No interfacial cracks, peeling off, tearing, break or slip of the particles is observed during all scratch tests for such high level of stresses, which indicates that particles do not fracture and are pushed into the matrix, as expected from the

**Figure 3.** AFM measurement (height map) of the top surface of the Ni-SiC coating (left) and a 2D height profile of the surface (right) after OP-U polishing.**Figure 4.** Profiles from nanoscratch test in correlation with an optical microscopic observation of the residual groove.

literature [28,29]. These experimental observations suggest a strong adhesion between the SiC particles and the Ni matrix. This high interfacial mechanical strength indicates a good quality of the interface, ensuring a stress transfer between the two phases inside the coating.

### Mechanical properties from nanoindentation tests

Mechanical properties of the PRMMC coating and of the reference samples were determined from nanoindentation tests following the method of Oliver and Pharr [14]. An average maximum load of  $(285 \pm 14)$  mN is reached at 2  $\mu\text{m}$  indentation depth. Poisson's coefficients of 0.3, 0.31 and 0.17 were used for elastic moduli calculations of, respectively, the Ni-SiC coating, Ni and  $\alpha$ -SiC samples. Hardness and elastic modulus evolutions are displayed in Figure 5 as a function

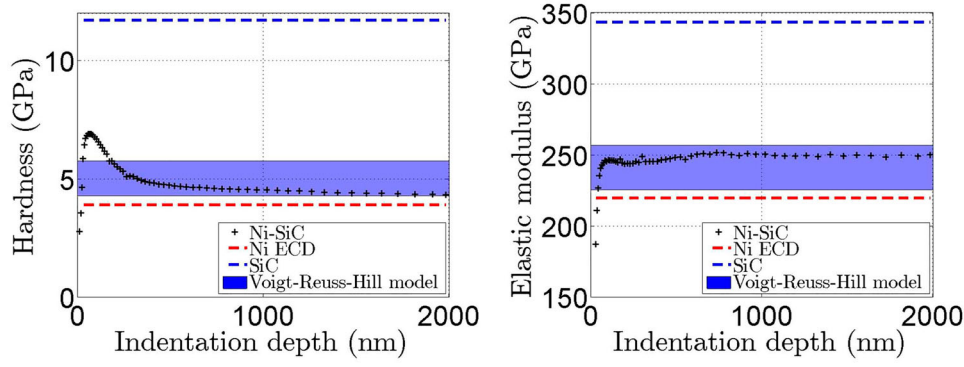


**Figure 5.** Hardness (left) and modulus of elasticity (right) as a function of indentation depth for the different samples and comparison with predictions from the Voigt–Reuss–Hill model.

of the indentation depth for each sample. No substrate effect is observed at high displacement, as expected considering that the maximum indentation depth normalised by the coating thickness is about 1.1%, which is well below the 10% empirical rule, proposed by Fischer-Cripps [30]. In the case of composite material, it is possible to bound mechanical properties using rules of mixture [31,32]. Simple Voigt (isostrain) and Reuss (isostress) models are given, respectively, by Equations (1) and (2). Usually, the Voigt–Reuss–Hill model is used and gives a good approximation for polycrystalline and composite materials (Equation (3)).

$$X_{C,Voigt} = f_p X_p + f_M X_M \quad (1)$$

$$X_{C,Reuss} = \frac{f_M X_M}{f_p X_p + f_M X_M} \quad (2)$$

$$X_{C,Voigt-Reuss-Hill} = \frac{X_{C,Voigt} + X_{C,Reuss}}{2} \quad (3)$$

with  $X_C$ ,  $X_p$ ,  $X_M$ , respectively, mechanical property (hardness or elastic modulus) of the composite material, the particles and the matrix, and  $f_p$  and  $f_M$ , the volume fraction of particles and matrix. Assuming that surface fractions given in Table 1 are equivalent to volume fractions, composite properties values are estimated by using surface fraction values of each phase (obtained by EBSD) and hardness and elastic modulus values of the Ni and  $\alpha$ -SiC (Table 2), in Equations (1) and (2). Voigt–Reuss–Hill domains are obtained with Equation (3)

**Table 2.** Mean values of hardness and modulus of elasticity for Ni–SiC sample and for Ni and bulk SiC references.

	Hardness (GPa)	Elastic modulus (GPa)
Ni coating reference	$3.9 \pm 0.3$	$219.7 \pm 7.2$
$\alpha$ -SiC reference	$11.7 \pm 3.0$	$343.2 \pm 50.0$
Ni–SiC coating	$5.2 \pm 1.3$	$247.2 \pm 8.0$
Voigt's model (Equation(1))	$5.5 \pm 1.0$	$245.4 \pm 18.2$
Reuss's model (Equation (2))	$4.5 \pm 0.5$	$237.0 \pm 13.3$
Voigt–Reuss–Hill model (Equation (3))	$5.0 \pm 0.7$	$241.1 \pm 15.7$

and are plotted in Figure 5 for both hardness and elastic modulus, from the minimum and maximum composite properties deduced from Equations (1) and (2). It is clear from Figure 5 that the Voigt–Reuss–Hill model bounds elastic and plastic properties of Ni–SiC coating. The composite coating is 33% harder and 12.5% stiffer than the Ni coating reference, which emphasises the metallic matrix reinforcement and which is in agreement with the literature. The composite coating is 33% harder and 12.5% stiffer than the Ni coating reference, which emphasises the metallic matrix reinforcement and which is in agreement with the literature [33–35]. However, according to the literature [36], such hardening effect may be the result of simultaneous phenomenon like an inherent flow behaviour (dislocations generation and interaction) and of the incorporation of hard dispersed particles (interaction between dislocations and particles/matrix interface).

Finally, the complex mechanical behaviour observed for such coating during nanoindentation at small indentation depths ( $< 250$  nm) could be accounted for by indentation size effects, and particularly in the case of Ni electroplated at a current density higher than  $2 \text{ A/dm}^2$ , according to Delobelle [37], by surface effect (roughness, surface topography, tip defect, etc.), and/or surface work hardening given the surface preparation (mechanical–chemical polishing). Thus, average mechanical properties are calculated for indentation depths between 250 and  $2 \mu\text{m}$  (Table 2) and compared to calculated mechanical properties using the different rules of mixtures. Note that the obtained values for the nanocrystalline Ni are consistent with the literature [37] and that mean hardness and elastic modulus values calculated with the Voigt–Reuss–Hill model are, respectively, 96% and 97% of the experimental average mechanical properties of the different phases.

### Mapping of mechanical properties

Determination of the mechanical properties of each individual phase in the case of a composite coating

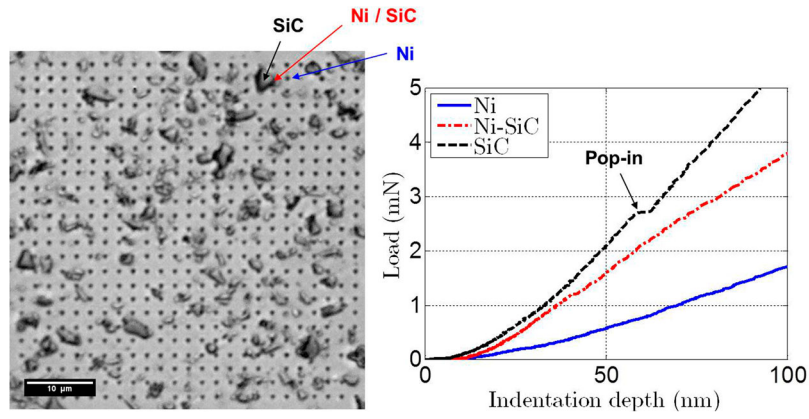


**Figure 6.** Optical microscopic observation of indentation grid on the Ni-SiC top surface (on the left) and load-displacement curves corresponding to selected indents (on the right).

can be achieved using the grid nanoindentation technique [17–19,21]. Microscopic observation of the  $25 \times 25$  nanoindents grid is shown in Figure 6 together with load-displacement curves obtained for selected indents on the Ni matrix, on a SiC particle and on a Ni/SiC interface. Mechanical property maps obtained from this nanoindentation grid experiment are plotted in Figure 7, using a Matlab routine from Mercier et al. [21]. Linear interpolation and smoothing steps are applied on the raw dataset in order to lessen pixelization effect and noise from the measurement, to get cleaner and more readable maps. Moreover, visual discrimination between phases is facilitated by plotting isosurfaces from these interpolated and smoothed experimental results. These maps obtained for the Ni-SiC coating are then overlaid (70% of transparency) to the micrographs of the grid (Figure 7). A good correlation is found between the peaks of the hardness or elastic modulus maps and the presence of SiC particles. Then, an ICBTI analysis of these experiments is proposed to extract mean mechanical property values and mean phase fractions (Figure 8), using a Matlab

toolbox [38]. A threshold is applied on the mechanical and microstructural maps before being binarized. The microstructural map thresholding is based on grey-scale distribution of the micrograph, while for the mechanical property maps thresholding is based on the phase distribution. For mechanical property map, threshold values are obtained by finding the intermediate value between matrix and particle peaks, while respecting phase ratios given in Table 1. Threshold values are found to be  $E_{thr} = 238.9$  GPa and  $H_{thr} = 6.4$  GPa, respectively, for the elastic modulus and hardness maps. After thresholding and binarization operations, the difference between binarized mechanical property and microstructural maps is computed and plotted so as to create correlation maps. This procedure is described graphically in Figure 8. Mechanical property-microstructure correlation maps allow assessing the match between indents and the probed phase in order to select indents representative for each single phase. Then, the intersection between these two mechanical properties-microstructure correlation maps gives a new correlation map without measurements

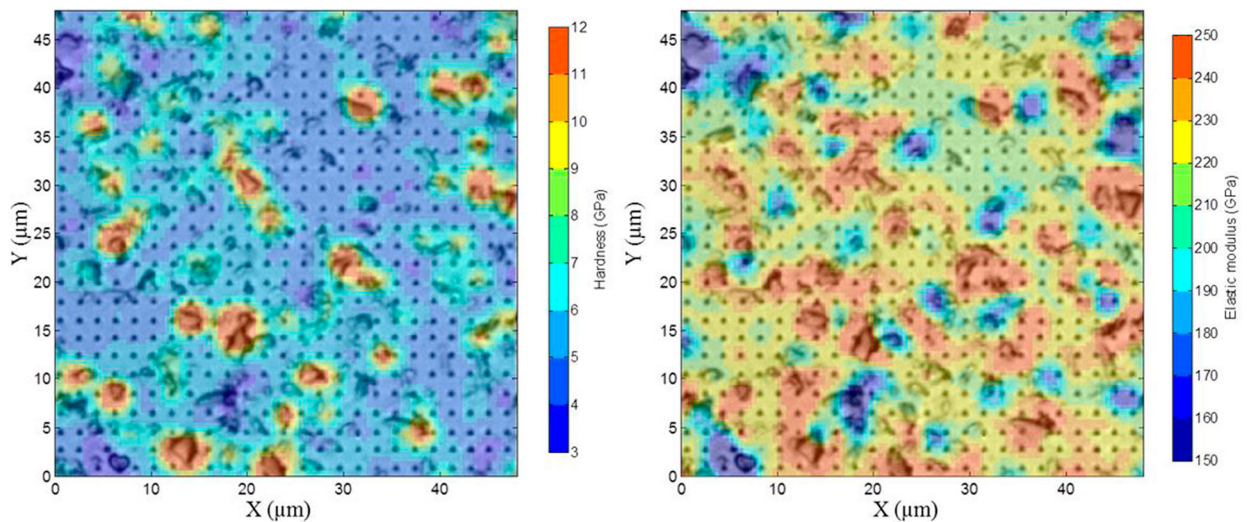


**Figure 7.** Overlay of hardness (on the left) and modulus of elasticity (on the right) maps with the optical microscopic observation of indentation grid on the Ni-SiC top surface (overlay with 70% transparency).



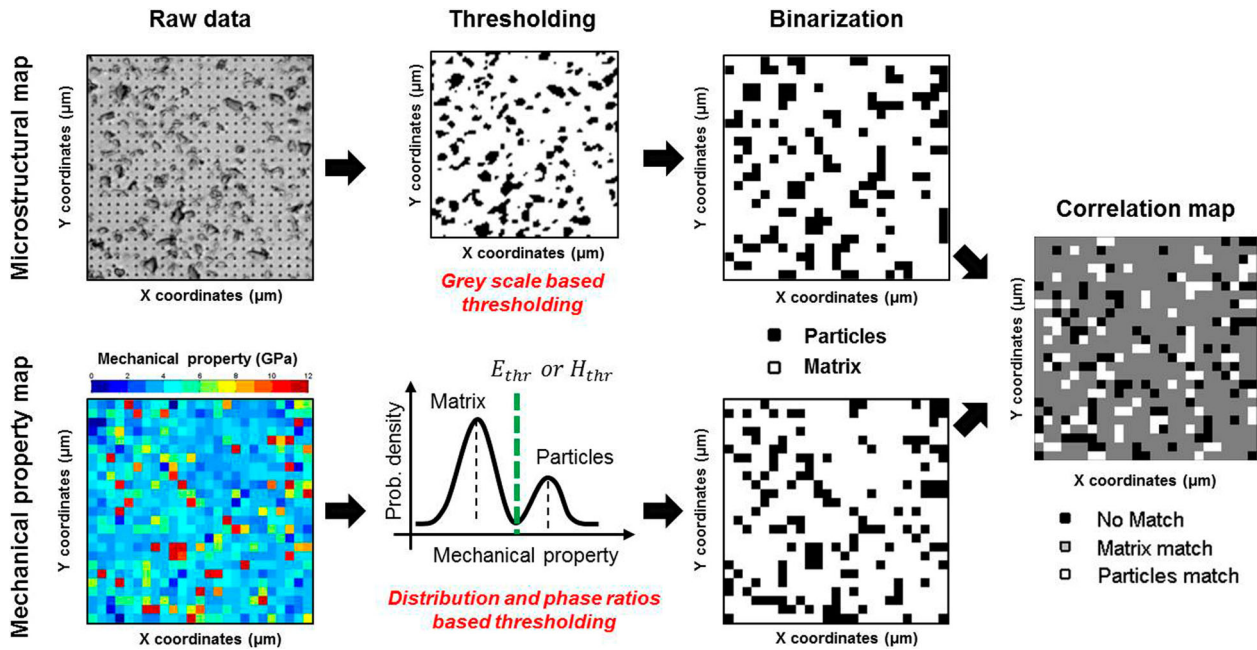


**Figure 8.** Principle of the ICTBI analysis, with thresholding and binarization steps.

artefacts (Figure 9). Such abnormal measurements may come from the presence of a defect (void, crack, surface pollution, etc.) or from the detection of an underlying or very small particle. The procedure is applied to the Ni-SiC sample (Figure 10) and correlation indices are found

to be 70% and 71%, respectively, for elastic modulus – microstructure and hardness – microstructure maps (Figure 10(b, c)). The mechanical property correlation map generated from these mechanical properties – microstructure maps (Figure 10(d)) gives average

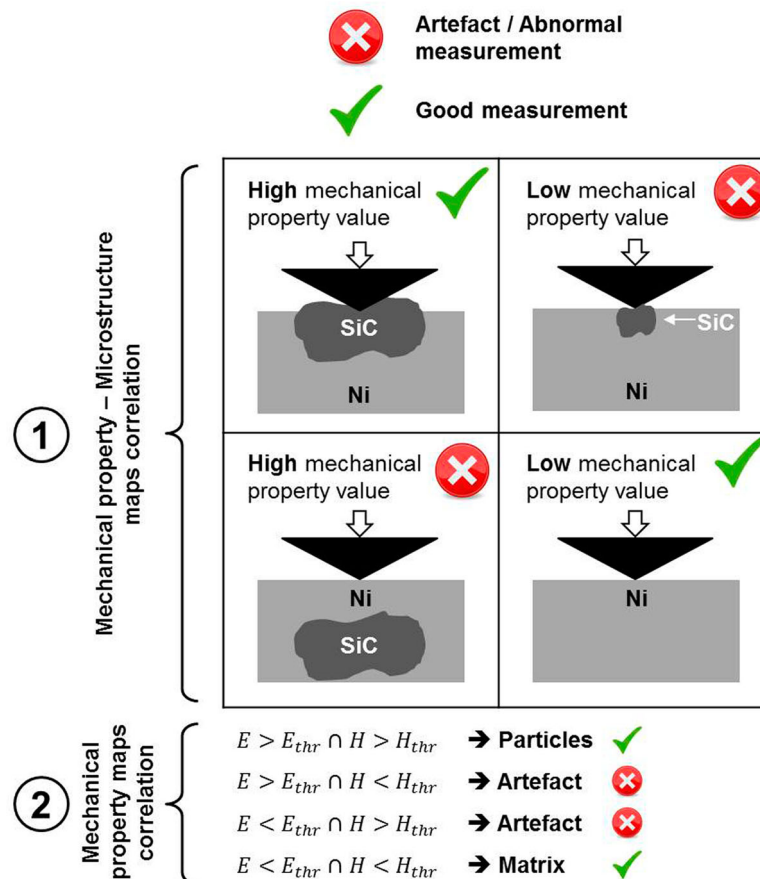


**Figure 9.** Schematisation of different indentation tests (cross-sectional view) and mathematical criteria, for discrimination between correct measurements and artefacts in the correlation process during the ICTBI analysis.

mechanical property values (Figure 10(e)), which are normalised with obtained values from nanoindentation for reference samples given in Table 2 and summarised in Tables 3 and 4. With this ICBTI method, normalised mechanical property values are comprised between 0.83 and 1.15, in good agreement respectively with values from Table 2.

This analysis emphasises the fact that, it is possible to facilitate direct quantification of the mechanical properties of each phase, by applying an automatic statistical treatment to identify the indents matching with the observed microstructure, when indent size is

much lower than the average microstructure size (here mean Ni grain clusters and mean SiC particles radius (Figure 9)). From this new way to analyse nanoindentation grid experiments, it is possible to consider only indentation tests corresponding to the probed microstructure and thus to exclude measurement artefacts (too small particles or underlying particles in the metallic matrix) which allows for a more reliable quantification of the mechanical properties of each phase. Such mapping allows also highlighting the hardness or elastic modulus difference between the metallic matrix and the ceramic particles. Thus, a

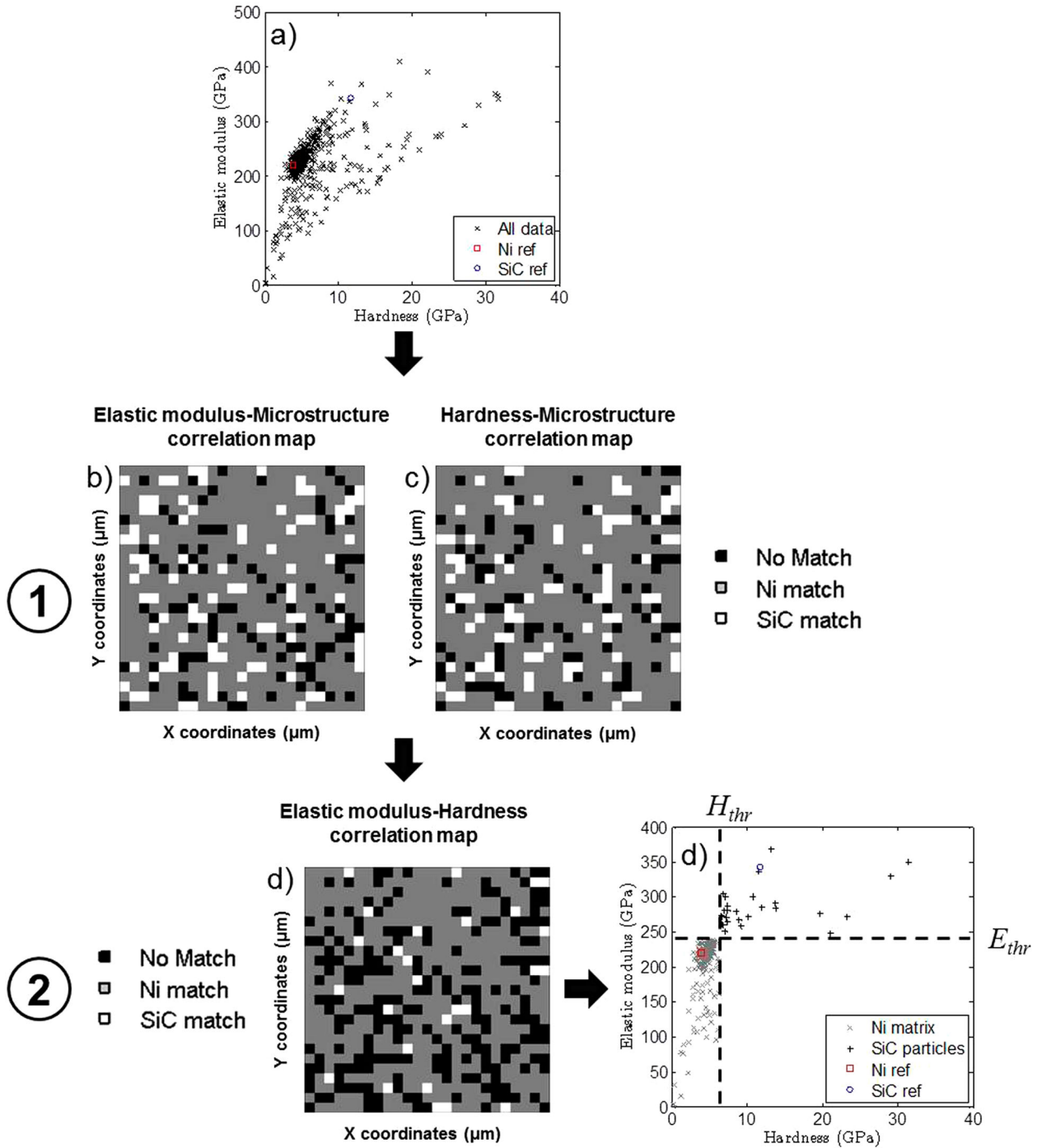


**Figure 10.** a) Plot of elastic modulus vs. hardness values obtained for all indents, used for the correlation maps generation (b) for elastic modulus and (c) for hardness). (d) Mechanical property correlation map obtained by the intersection of the (b) and (c) maps, giving (e) the plot of elastic modulus vs hardness values, without artefact or abnormal measurements.

**Table 3.** Mean values of phase fraction and hardness of Ni, SiC and Ni/SiC interface, obtained from ICBTI and from deconvolution of bi- and tri-modal Gaussian distribution.

		Ni (#1)	Ni/SiC interface (#2)	SiC (#3)
ICBTI (Figure 10)	Hardness	$(4.5 \pm 0.9)$ GPa	–	$(11.8 \pm 7.0)$ GPa
	Normalised hardness	115%	–	101%
Bimodal distribution (Figure 11(a))	Phase fraction	78%	–	22%
Trimodal distribution (Figure 11(b))	Hardness	$(4.5 \pm 0.5)$ GPa	$(6.7 \pm 1.2)$ GPa	$(11.3 \pm 0.7)$ GPa
	Normalised hardness	115%	–	97%

**Table 4.** Mean values of phase fraction and modulus of elasticity of Ni, SiC and Ni/SiC interface, obtained from ICBTI and from deconvolution of bi- and tri-modal Gaussian distribution.

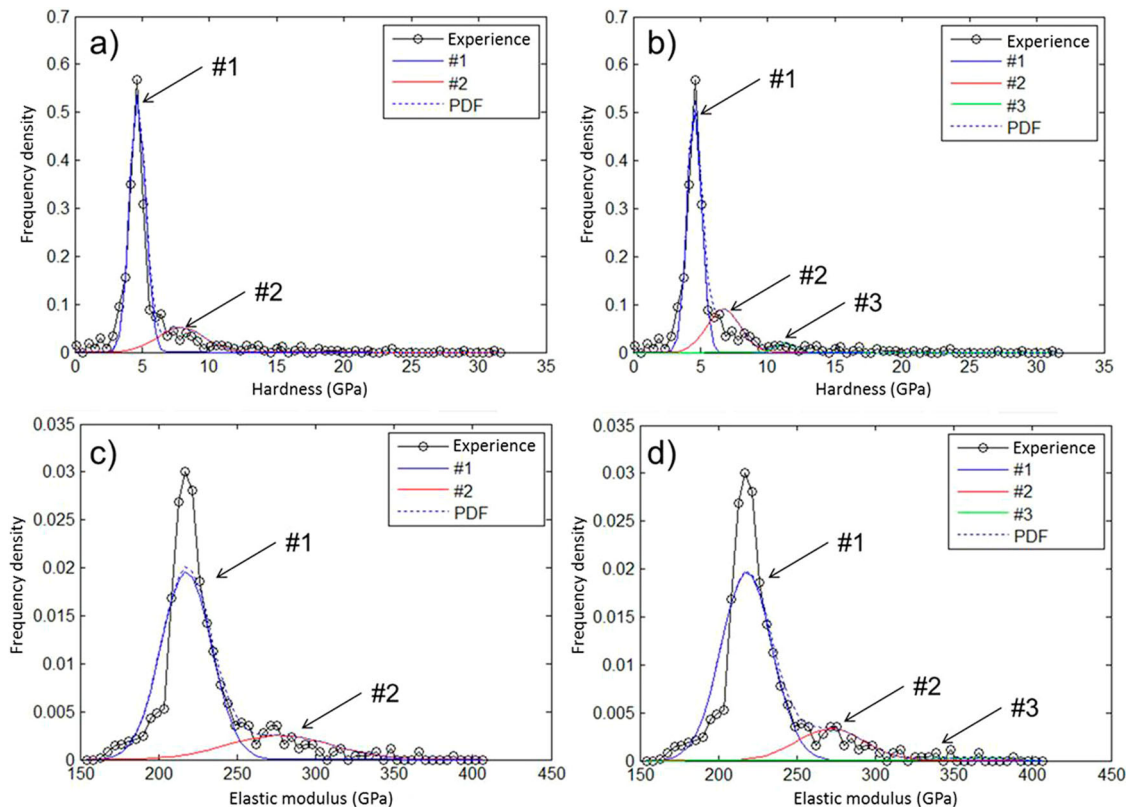
		Ni (#1)	Ni/SiC interface (#2)	SiC (#3)
ICBTI (Figure 10)	Elastic modulus	$(209.9 \pm 37.5)$ GPa	–	$(286.3 \pm 29.8)$ GPa
	Normalised elastic modulus	96%	–	83%
Bimodal distribution (Figure 11(a))	Phase fraction	80%	–	20%
Trimodal distribution (Figure 11(b))	Elastic modulus	$(218.0 \pm 16.3)$ GPa	$(271.6 \pm 21.4)$ GPa	$(360.5 \pm 22.8)$ GPa
	Normalised elastic modulus	99%	–	105%

great interest to plot such nanoindentation maps is found for visualisation of interface effects and mechanical characterisation of heterogeneous materials.

### Statistical distribution of mechanical properties

Mechanical properties of each coating constituent can be extracted by a statistical analysis of nanoindentation results. Matlab code has been used [38] to plot probability function of hardness and elastic modulus values

(Figure 11). Probability densities follow a Gaussian mixture model and are analytically fitted with tri- or bimodal distributions. The trimodal distribution takes into account the non-negligible effect of the Ni–SiC interfaces [39,40,21,41], but also minimises an apparent softening of the hard particles and an apparent hardening/stiffening of the metallic matrix [42–45,46]. Based on this, the mean phase fractions were estimated for the Ni and the SiC under the assumption of a bimodal distribution, while mean mechanical property values of Ni,

**Figure 11.** Deconvolution of hardness and modulus of elasticity frequency plots, under the assumption of bimodal (a and c) and trimodal distributions (b and d).

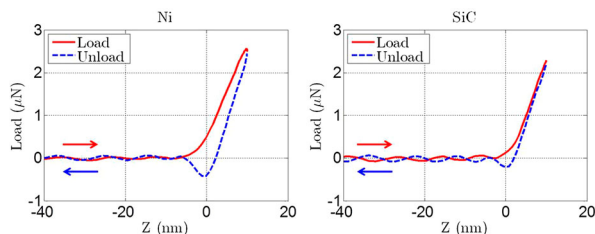


**Figure 12.** Typical curves of force as a function of vertical displacement for Ni (left) and SiC (right).

SiC and Ni/SiC interface were estimated under the assumption of a trimodal distribution, by Gaussian mixture decomposition (Tables 3 and 4). Hardness and elastic modulus mean values are then normalised with obtained values from nanoindentation for reference samples given in Table 2. This analysis bears out results obtained with ICBTI analysis and demonstrates that a good estimation of the phase fractions can be achieved when probability density functions are fitted with Gaussian bimodal distribution, while the mechanical properties are better assessed using trimodal distribution.

### Investigation of mechanical properties by PF-QNM

Given the difficulty of applying conventional methods (e.g. nanoindentation) for mechanical characterisation of such coatings, PF-QNM experiments were conducted on the Ni–SiC coating. Typical experimental curves of force as a function of vertical displacement are shown in Figure 12 for Ni and SiC phases. For both samples, the red solid line represents the measured force on the probe during the approach of the tip to the sample (load), and the blue-dashed line represents the force, while the tip moves away from the sample (unload). Load and unload parts of the SiC force curve are overlaid, while a hysteresis (deformation) is observed for the Ni phase, with a deeper negative force peak (adhesion) at the end of the unload process. This behaviour comes from a greater tip penetration (with inelastic deformation) into the material and is specific to soft and compliant phases. The contact area between the tip and the sample is also increasing for the Ni phase implying higher adhesion forces, with about 0.45  $\mu\text{N}$  for the Ni and 0.2  $\mu\text{N}$  for the SiC. It is clear from these experiments that Ni matrix has an elastic–plastic behaviour and SiC particles are purely elastic. Unfortunately, these PF-QNM experiments were not successful for elastic modulus extraction and properties mapping for both phases. It may be due to the fact that stiffness of steel cantilever was not stiff enough compared to Ni and SiC phases. It is proposed in the future to use sapphire cantilever, which presents higher stiffness ( $> 500 \text{ N/m}$ ).

## Conclusion

The present work is devoted to the microstructural and mechanical characterisation of an electroplated Ni–SiC composite coating. By combining information from SEM, EDS and EBSD techniques, the coating is shown to consist of around 80% of Ni matrix with an average grain size of  $(0.34 \pm 0.27) \mu\text{m}$  and 20% of homogeneously distributed SiC particles of mean size  $(1.13 \pm 0.16) \mu\text{m}$ . Cohesion between the metal and ceramic phases was investigated using the nanoscratch technique. No sliding or tearing-off of the particles was observed during this test, which confirms the strength of the Ni/SiC interface and, hence the stress transfer from one phase to the other. Hardness and elastic modulus of the particle reinforced metallic matrix composite (PRMMC) were assessed at the composite scale as well as the scale of each individual phase based on statistical analysis of grid indentation data. Hardness and elastic modulus data were compared to predictions from simple rules of mixtures. Mechanical property maps were built and were quantitatively correlated to the microstructure map. Then, phase volume fractions and mechanical properties of each individual phase were extracted using ICBTI analysis and fit of probability distribution plots. The ICBTI method is a new way to analyse nanoindentation grid dataset by applying an automatic correlation procedure between mechanical property and microstructure maps, and leading to the exclusion of measurement artefacts and to a more reliable quantification of the mechanical properties of each phase. Finally, force–displacement curves obtained by PF-QNM highlighted elastic–plastic and elastic behaviours, respectively, for the Ni and SiC phases and provided in addition adhesion forces.

## Disclosure statement

No potential conflict of interest was reported by the authors.

## Funding

This work was supported by FP7 People: Marie-Curie Actions [Grant Number INDMAT (1510385)]. The authors would like to thank the Walloon region for financial support in the frame of the INDMAT project (BEWARE FELLOWSHIPS), co-funded by the European Union (FP7 – Marie-Curie Actions) and NoChrome project, funded in the frame of the ‘Recherche Collective 2013’ program. The authors would also like to thank EU for financial support in the frame of the ‘CLEARZINC/CLEARZINC SEM-FEG’ project (2007–2013 FEDER programs).

## ORCID

David Mercier  <http://orcid.org/0000-0003-1996-198X>  
Xavier Vanden Eynde  <http://orcid.org/0000-0002-4408-9540>



## References

- [1] Ibrahim IA, Mohamed FA, Lavernia EJ. Particulate reinforced metal matrix composites – a review. *J Mater Sci.* **1991**;26:1137–1156.
- [2] Chawla N, Shen Y-L. Mechanical behavior of particle reinforced metal matrix composites. *Adv Eng Mater.* **2001**;3:357–370.
- [3] Walsh FC, de Leon CP. A review of the electrodeposition of metal matrix composite coatings by inclusion of particles in a metal layer: an established and diversifying technology. *Trans IMF.* **2014**;92:83–98.
- [4] Nieto A, Bisht A, Lahiri D, et al. Graphene reinforced metal and ceramic matrix composites: a review. *Int Mater Rev.* **2017**;62:241–302.
- [5] Maurin G, Lavanant A. Electrodeposition of nickel/silicon carbide composite coatings on a rotating disc electrode. *J Appl Electrochem.* **1995**;25:1113–1121.
- [6] Lee H-K, Lee H-Y, Jeon J-M. Codeposition of micro- and nano-sized SiC particles in the nickel matrix composite coatings obtained by electroplating. *Surf Coat Technol.* **2007**;201:4711–4717.
- [7] Vaezi MR, Sadrnezhaad SK, Nikzad L. Electrodeposition of Ni–SiC nano-composite coatings and evaluation of wear and corrosion resistance and electroplating characteristics. *Colloids Surf Physicochem Eng Asp.* **2008**;315:176–182.
- [8] Walsh FC, Low CTJ, Bello JO. Influence of surfactants on electrodeposition of a Ni-nanoparticulate SiC composite coating. *Trans IMF.* **2015**;93:147–156.
- [9] Miguel FL, Müller R, Mathur S, et al. Microstructure and mechanical properties of electrodeposited Ni and Ni-matrix-nanocomposite thin films. *Mater Sci Eng A.* **2015**;646:254–262.
- [10] Miracle DB. Metal matrix composites – from science to technological significance. *Compos Sci Technol.* **2005**;65:2526–2540.
- [11] Lampke T, Wielage B, Dietrich D, et al. Details of crystalline growth in co-deposited electroplated nickel films with hard (nano)particles. *Appl Surf Sci.* **2006**;253:2399–2408.
- [12] Chawla KK. Interfaces in metal matrix composites. *Compos Interfaces.* **1996**;4:287–298.
- [13] Pöhl F, Schwarz S, Junker P, et al. Indentation and scratch testing—experiment and simulation. *Int. Conf. Stone Concr. Mach. ICSCM* [Internet]. 2015 [cited 2015 Dec 8]. p. 292–308. Available from: <http://134.147.247.26/ojs/index.php/ICSCM/article/download/412/368>
- [14] Oliver WC, Pharr GM. An improved technique for determining hardness and elastic modulus using load and displacement sensing indentation experiments. *J Mater Res.* **1992**;7:1564–1583.
- [15] Dirras G, Gubicza J, Ramtani S, et al. Microstructure and mechanical characteristics of bulk polycrystalline Ni consolidated from blends of powders with different particle size. *Mater Sci Eng A.* **2010**;527:1206–1214.
- [16] Dong S, Beake BD, Parkinson R, et al. Determination of hardness and young's modulus of brush plated nano-Al<sub>2</sub>O<sub>3</sub>/Ni composite coating by nanoindentation testing. *Surf Eng.* **2003**;19:195–199.
- [17] Constantinides G, Ravi Chandran KS, Ulm F-J, et al. Grid indentation analysis of composite microstructure and mechanics: principles and validation. *Mater Sci Eng A.* **2006**;430:189–202.
- [18] Randall NX, Vandamme M, Ulm F-J. Nanoindentation analysis as a two-dimensional tool for mapping the mechanical properties of complex surfaces. *J Mater Res.* **2009**;24:679–690.
- [19] [19] Němeček J. Nanoindentation of heterogeneous structural materials [Internet] [PhD thesis]. Czech Technical University; 2009 [cited 2015 Apr 16]. Available from: [http://ksm.fsv.cvut.cz/~nemecek/teaching/dmpo/literatura/habilitation%20thesis\\_Nemecek\\_CTU-01-2010.pdf](http://ksm.fsv.cvut.cz/~nemecek/teaching/dmpo/literatura/habilitation%20thesis_Nemecek_CTU-01-2010.pdf)
- [20] Yang H, Wang Z, Zhang H, et al. Microstructure and nanoindentation behaviour of Ni surface modified Ti<sub>6</sub>Al<sub>4</sub>V. *Surf. Eng.* **2015**;31:923–929.
- [21] Mercier D, Vanhumbecq J-F, Caruso M, et al. Caractérisation mécanique par nanoindentation d'un revêtement composite à matrice nickel électrodéposé. *Matér Tech.* **2017**;105:106.
- [22] Dhakar B, Chatterjee S, Sabiruddin K. Measuring mechanical properties of plasma-sprayed alumina coatings by nanoindentation technique. *Mater Sci Technol.* **2016**;33(3):1–9.
- [23] Wilson W, Sorelli L, Taghit-Hamou A. Automated coupling of NanoIndentation and Quantitative Energy-Dispersive Spectroscopy (NI-QEDS): A comprehensive method to disclose the micro-chemo-mechanical properties of cement pastes. *Cem. Concr. Res.* [Internet]. 2017 [cited 2017 Oct 16]; Available from: <http://www.sciencedirect.com/science/article/pii/S0008884617305549>
- [24] Young TJ, Monclus MA, Burnett TL, et al. The use of the PeakForce™ quantitative nanomechanical mapping AFM-based method for high-resolution Young's modulus measurement of polymers. *Meas Sci Technol.* **2011**;22:125703.
- [25] Trtik P, Kaufmann J, Volz U. On the use of peak-force tapping atomic force microscopy for quantification of the local elastic modulus in hardened cement paste. *Cem Concr Res.* **2012**;42:215–221.
- [26] Morales-Rivas L, González-Orive A, Garcia-Mateo C, et al. Nanomechanical characterization of nanostructured bainitic steel: Peak Force Microscopy and Nanoindentation with AFM. *Sci. Rep.* [Internet]. 2015 [cited 2016 Feb 12];5. Available from: <http://www.ncbi.nlm.nih.gov/pmc/articles/PMC4658537/>
- [27] Beake BD, Harris AJ, Liskiewicz TW. Review of recent progress in nanoscratch testing. *Tribol – Mater Surf Interfaces.* **2013**;7:87–96. <https://doi.org/10.1179/1751584X13Y.0000000037>
- [28] Huang L, Topping TD, Yang H, et al. Nanoscratch-induced deformation behaviour in B4C particle reinforced ultrafine grained Al alloy composites: a novel diagnostic approach. *Philos Mag.* **2014**;94:1754–1763.
- [29] Zikin A, Badisch E, Hussainova I, et al. Characterisation of TiC–NiMo reinforced Ni-based hardfacing. *Surf Coat Technol.* **2013**;236:36–44.
- [30] Fischer-Cripps AC. Nanoindentation [Internet]. 3rd ed. Springer; 2011. Available from: <http://dx.doi.org/10.1007/978-1-4419-9872-9>
- [31] Meyers M, Chawla K. Mechanical Behavior of Materials [Internet]. Second edition. Cambridge University Press; 2008 [cited 2016 Aug 9]. Available from: <http://www.cambridge.org/be/academic/subjects/engineering/materials-science/mechanical-behavior-materials-2nd-edition?format=HB&isbn=9780521866750>
- [32] Wasekar NP, Latha SM, Ramakrishna M, et al. Pulsed electrodeposition and mechanical properties of Ni–W/SiC nano-composite coatings. *Mater Des.* **2016**;112:140–150.

- [33] Kim HS. On the rule of mixtures for the hardness of particle reinforced composites. *Mater Sci Eng A*. 2000;289:30–33.
- [34] Kim HS, Hong SI, Kim SJ. On the rule of mixtures for predicting the mechanical properties of composites with homogeneously distributed soft and hard particles. *J Mater Process Technol*. 2001;112:109–113.
- [35] Shoukry SN, Prucz JC, Shankaranarayana PG, et al. Microstructure modeling of particulate reinforced metal matrix composites. *Mech Adv Mater Struct*. 2007;14:499–510.
- [36] Chatterjee S, Chabri S, Chakraborty H, et al. Micromechanical and nanoscratch behavior of SiCp dispersed metal matrix composites. *J Mater Eng Perform*. 2015;24:3407–3418.
- [37] Delobelle P, Richard F, Qasmi M. Quelques potentialités de l'essai de nanoindentation. Cas du nickel polycristallin et électrodéposé : interprétation du module d'indentation, de la dureté, des effets d'échelle et des paramètres d'identification inverse. *Matér Tech*. 2008;96:83–94.
- [38] Němeček J, Králík V, Vondřejc J. Micromechanical analysis of heterogeneous structural materials. *Cem Concr Compos*. 2013;36:85–92.
- [39] Haušild P, Materna A, Kocmanová L, et al. Determination of the individual phase properties from the measured grid indentation data. *J Mater Res*. 2016;31(22):1–11. <https://doi.org/10.1557/jmr.2016.375>
- [40] de Vasconcelos LS, Xu R, Li J, et al. Grid indentation analysis of mechanical properties of composite electrodes in Li-ion batteries. *Extreme Mech. Lett.* [Internet]. 2016 [cited 2016 Mar 14]; Available from: <http://www.sciencedirect.com/science/article/pii/S2352431616300190>
- [41] Čech J, Haušild P, Materna A, et al. Approche statistique pour identifier les propriétés mécaniques des phases individuelles à partir de données d'indentation. *Matériaux & Techniques*. 2017;105(1):1–7. <https://doi.org/10.1051/mattech/2016041>
- [42] Shen Y-L, Guo YL. Indentation modelling of heterogeneous materials. *Model Simul Mater Sci Eng*. 2001;9:391–398.
- [43] Durst K, Goken M, Vehoff H. Finite element study for nanoindentation measurements on two-phase materials. *J Mater Res*. 2004;19:85–93.
- [44] Yan W, Pun CL, Wu Z, et al. Some issues on nanoindentation method to measure the elastic modulus of particles in composites. *Compos Part B Eng*. 2011;42:2093–2097.
- [45] Low TF. A numerical study on the nanoindentation response of a particle embedded in a matrix [Internet] [PhD thesis]. Monash University. Faculty of Engineering. Department of Mechanical and Aerospace Engineering; 2014 [cited 2015 Nov 18]. Available from: [http://arrow.monash.edu.au/vital/access/manager/Repository/monash:128757?exact=sm\\_subject%3A%22Nanoindentation%22](http://arrow.monash.edu.au/vital/access/manager/Repository/monash:128757?exact=sm_subject%3A%22Nanoindentation%22)
- [46] Yuan Z, Li F, Zhang P, et al. Mechanical properties study of particles reinforced aluminum matrix composites by micro-indentation experiments. *Chin J Aeronaut*. 2014;27:397–406.